Jour. Fac. Sci., Hokkaido Univ., Ser. VII (Geophysics), Vol. 10, No. 1, 1-19, 1996.

S-Wave Spectra from Strong Motion Seismograms: Source Parameters and Site Response

Abbas Mahdavian* and Tsutomu Sasatani

Division of Earth and Planetary Sciences, Graduate School of Science, Hokkaido University, Sapporo 060, Japan

(Received November 16, 1995)

Abstract

We analyze S-wave spectra from strong motion seismograms observed at the rock and sedimentary sites. The data are horizontal component records from earthquakes occurring in the southern part of Hokkaido, Japan (the magnitude range is 4 to 7.8 and the depth range, 40 to 130 km). These records were obtained by wide frequency band instruments. The S-wave spectra at the rock site for moderate-size events satisfactorily fit the omega-squared model after correction of spectral decay at high frequencies due to attenuation. Source parameters (seismic moments and corner frequencies) are obtained from the spectra by an objective method. They satisfy the scaling law with an average stress drop of about 200 bars. On the other hand, the S-wave spectra at the sedimentary site have a peak in the frequency range of 0.1 to a few Hz, in contrast with those at the rock site. We attribute the peak to a site response due to the thick sedimentary layer. The site response is estimated by averaging the residuals between the logarithms of the observed spectrum and the model spectrum calculated based on the scaling law.

The 1993 Kushiro-Oki earthquake ($M=7.8$) exhibits peculiar S-wave spectra even at the rock site. They have two corner frequencies which demonstrate a departure from the omega-squared model. This indicates a heterogeneous fault plane for this big event, and the second corner frequency, which is related to the scale-length of heterogeneities, is estimated at about 1 Hz. The heterogeneous rupture radiates abnormally strong short-period seismic waves; observed horizontal peak accelerations are much higher than those predicted by an empirical attenuation relation.

1. Introduction

The shape and amplitude of the Fourier amplitude spectrum of strong ground motion contain fundamental information about physical processes at the earthquake source and wave propagation in the earth. Many previous studies have supported the omega-squared source model from analysis of S-wave

* Present Affiliation: Mahab Ghodss Consulting Engineering, Zafar St., Takharestan St., Tehran, Iran.

strong ground motion (e.g., Hanks and McGuire, 1981; Rovelli et al., 1988; Takemura et al., 1991). However, several studies have shown observational evidences of departure from the omega-squared model (e.g., Izutani, 1984; Papageorgiou, 1988; Takemura et al., 1993). These S-wave spectra have two corner frequencies; the first corner frequency is related to the rupturing of the whole fault, while the second corner frequency is related to the average scale length of heterogeneities on a fault plane (e.g., Koyama, 1983).

Wave propagation effects, especially site response, also modify the spectrum radiated from the source. Site-dependent spectral shape have been observed in several studies (e.g., Rovelli et al., 1988; Humphery and Anderson, 1992). Frequency-dependent amplification is an important factor to predict strong ground motion (Boore, 1983; Mahdavian, 1993). Recently, source, propagation path, and local site effects in observed strong motion records are separated by an inversion method (e.g., Iwata and Irikura, 1988; Takemura et al., 1991). This method requires multiply recorded sets of earthquakes.

In this paper, we study S-wave spectra from strong motion seismograms based on data from earthquakes occurring in the southern part of Hokkaido, Japan. Since the number of observation sites is only two, it is inadequate to apply the inversion method. Here we study the S-wave spectra by assuming the omega-squared source model, and examine the dependence of the spectral shape on earthquake size and local geology.

2. Data

We study velocity seismograms observed at MYR and OUV in the Tokachi plain, Hokkaido, Japan (Fig. 1; Sasatani et al., 1990). The Tokachi plain is a sedimentary basin covered mainly by terrace deposits (Geological Survey of Hokkaido, 1980), which has the extent of about 100 km in the north-south direction and about 50 km in the east-west direction. MYR is located at the edge of the plain and strong motion seismometer is installed in the observational vault which was excavated in slate of the period of Mesozoic. OUV is located at the central part of the Tokachi plain and the seismometer is installed in a small cabin on the sediment. We refer to MYR and OUV as the rock site and the sedimentary site, respectively.

These stations consist of the velocity-type strong motion seismometer, VS-3, with a full scale range of 100 cm/s (Muramatu, 1977, 1995). The frequency characteristics of the seismometer are shown in Fig. 2. The VS-3 seismometer has a flat velocity response in the frequency range from about 0.002 up to about

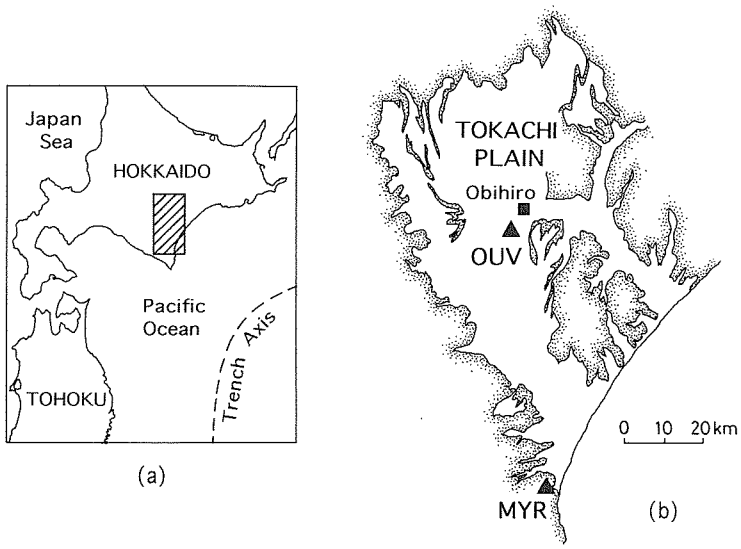

Fig. 1. (a) Map showing location of the Tokachi plain (shadowed region) in Hokkaido. (b) Simplified geological map of the Tokachi plain (revised from Geological Survey of Hokkaido, 1980) and strong motion observation stations (MYR and OUV). The Tokachi plain is covered mainly by Terrace deposits.

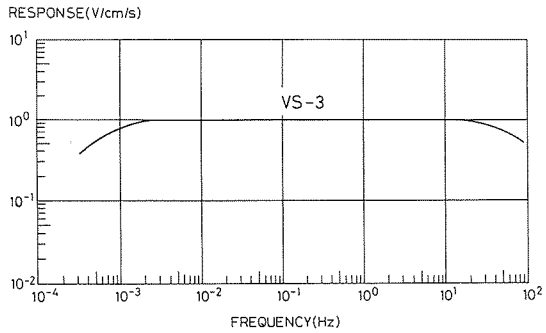

Fig. 2. Frequency characteristics of the velocity-type strong motion seismometer (Muramatu, 1977, 1995).

20Hz. The wide frequency band seismometer used here is necessary to obtain reliable information about S-wave spectrum of strong ground motion. The signals are digitized at a sampling frequency of 50 Hz and with a dynamic range of 16 bit. A corner frequency of anti-alias filter is set at 20 Hz.

In this study, we selected about 30 events among more than 100 earthquakes observed during the period of December, 1990 to August, 1992. This selection

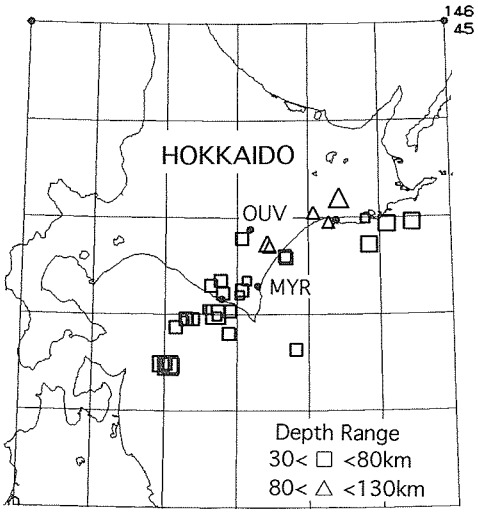

Fig. 3. Epicentral distribution of earthquakes analyzed in this study.

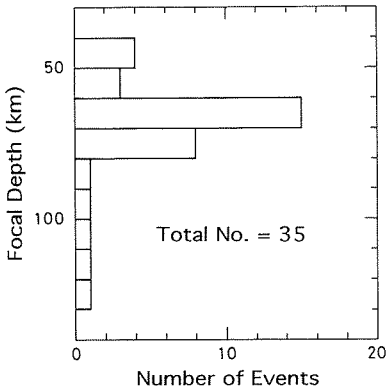

Fig. 4. Depth distribution of alalyzed earthquakes.

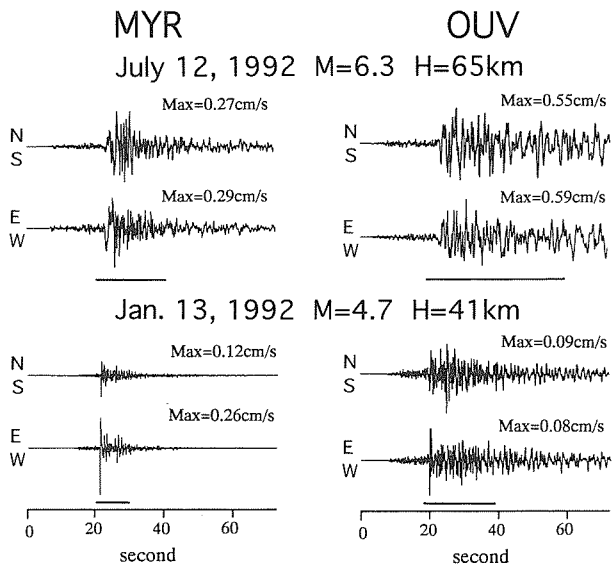

Fig. 5. An example of observed velocity seismograms at MYR (left) and OUV (right) stations. Bars indicate the S-wave portion used in the spectral analysis. The spectra for part of these seismograms are shown in Figs. 6 and 10.

was made based on the criteria ; 1) earthquakes producing seismograms with a high signal-to-noise ratio, and 2) those having hypocentral distances of less than 200 km. The latter criterion was imposed after the preliminary analysis of S-wave spectra. The reason is given in section 4.

Figure 3 shows the epicentral distribution of analyzed earthquakes whose list is given in Table 1. These events have a magnitude range of 3.7 to 6.4 and a depth range of 40 to 130 km (Fig. 4). The data set for moderate-size events consists of records from these events. Figure 5 shows an example of observed velocity seismograms. We can see different features of seismograms at MYR and OUV ; the seismograms at MYR are simply composed of S waves, but those at OUV show not only S-waves but also strong later phases.

More recently, the Kushiro-Oki earthquake with a magnitude of 7.8 occurred on January 15, 1993 at the depth of 107 km beneath Kushiro city, Hokkaido (see Fig. 11). The records from this big event are analyzed separately.

3. Method of analysis

We apply the Husid plot method to define the S-wave portion. First the acceleration seismogram is obtained by differentiating the velocity seismogram. Then we calculate the Husid plot from the acceleration seismogram and define the S-wave portion as the time needed to build-up between 5 to 95 percent of the Husid plot (Dobry et al., 1978). An example of the selected S-wave portions is shown in Fig. 5.

We analyze Fourier spectra for horizontal component seismograms using the above S-wave portion. Sampled data are windowed by 10 percent cosine tapering at both ends. The Fourier amplitude spectrum is calculated from the velocity seismogram and then it is transformed into displacement and acceleration spectra as the need arises. The S-wave portion may be contaminated by the P-coda. In order to check a signal-to-noise ratio, we compare the spectral amplitudes of P-coda and S-wave portion with the same window length. In this study, we use only seismograms with a high signal-to-noise ratio (greater than 4) selected through the comparison.

Based on the omega-squared source model (Aki, 1967 ; Brune, 1970 ; Hanks and McGuire, 1981) and an exponential spectral decay at high frequencies due to attenuation in the earth (Anderson and Hough, 1984), we assume the S-wave displacement spectrum $D(f)$ as follows :

$$D(f)=\frac{0.89M_0}{4\pi\rho\beta^3R}\frac{1}{[1+(f/f_0)^2]}\exp(-\pi\kappa f). \quad (1)$$

Here M_0 is the seismic moment, f_0 is the source corner frequency, κ is the spectral decay parameter, R is the source to station distance, ρ is the density, and β is the S-wave velocity. The constant, 0.89, account for the average S-wave radiation pattern (=0.63), amplification due to the free surface (=2), and partitioning of energy into the two horizontal components ($=1/\sqrt{2}$). In this study, it is assumed that $\rho=3.2$ g/cm^3 and $\beta=4.5$ km/sec.

The spectral decay parameters at MYR and OUV have been studied by Mahdavian and Sasatani (1994) for the same data set used in this study. They estimated κ value for each record based on the acceleration spectrum on log-linear plot (Anderson and Hough, 1984). Strictly speaking, the spectral decay parameter is an observational parameter, but it represents reasonably attenuation within the earth (Anderson and Hough, 1984). Hereafter we study the S-wave spectra corrected for the attenuation using κ values obtained by Mahdavian and Sasatani (1994, see their Table 1).

4. S-wave spectra for moderate-size events at the rock site

Figure 6 shows an example of S-wave displacement spectra at the rock site, MYR. They satisfactorily fit the omega-squared model; the spectra have a flat level at low frequencies and a fall-off proportional to f^{-2} in the frequency range higher than the corner frequency. Then we estimate the source parameters (M_0 and f_0) from those spectra by using the Andrews' objective method (1986). The results are summarized in Table 1. They are obtained an average from two horizontal components. As shown in Figs. 6(a) and (b), two horizontal components have approximately the same spectral shape, then give nearly the same source parameters.

In Fig. 7, we compare our estimates of M_0 for seven larger events in Table 2 with centroid moment tensor solutions of the Harvard University group, HRV (e.g., Dziewonski et al., 1983). We can see that our M_0 estimates for events with the hypocentral distance of less than about 200 km are the same as HRV estimates within a factor of 2. This indicates that our estimation method is reasonably good for these events. However, for events with the hypocentral distance of more than 200 km, our seismic moments are systematically lower than HRV solutions. This may mean that the simple formula (1) is not adequate for describing radiation of seismic waves from a distant source. Thus we

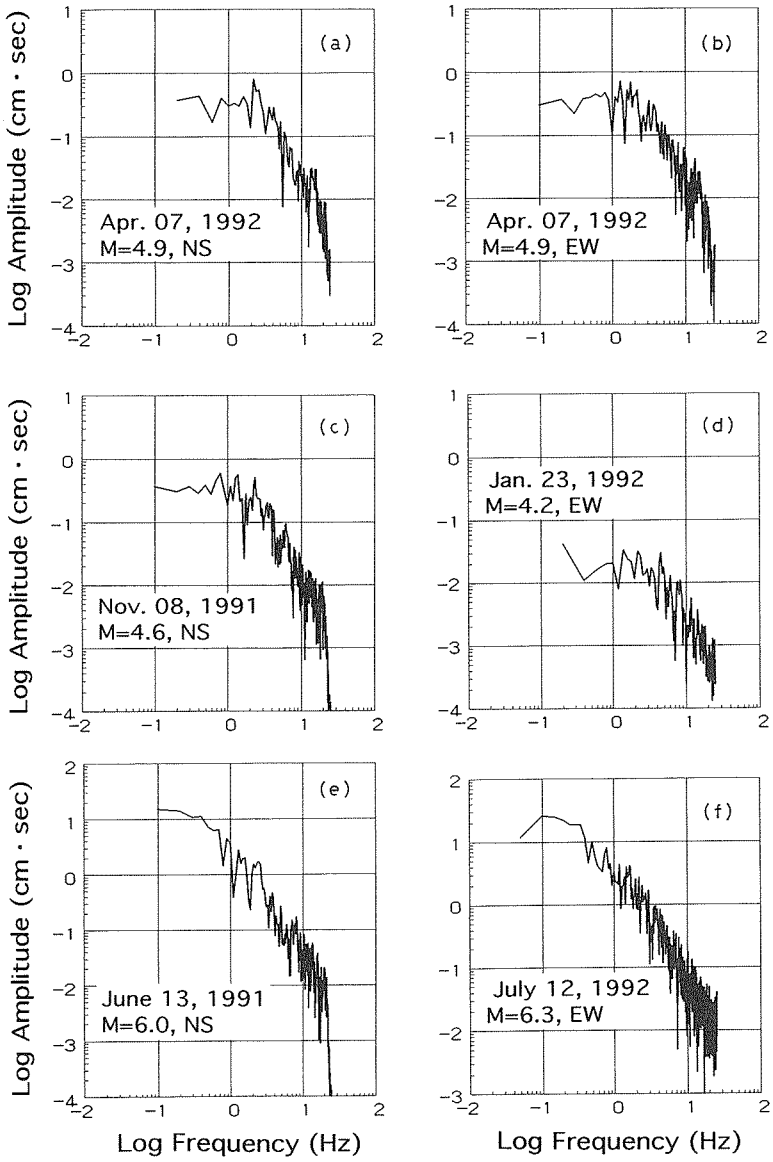

Fig. 6. An example of S-wave displacement spectra at MYR for moderate-size events.

Table 1. List of the analyzed moderate-size events. H, R, M_0 and f_0 indicate the focal depth, hypocentral distance, seismic moment and corner frequency, respectively.

No.	Date	Time	M	H (km)	R (MYR) (km)	R (OUV) (km)	$M_0 \times 10^{22}$ (dyn•cm)	f_0 (Hz)
1	90 Dec. 09	12 : 12	4.3	117	158	—	1.6	3.3
2	90 Dec. 10	16 : 27	5.1	44	196	—	35	1.5
3	90 Dec. 25	06 : 09	4.9	68	108	—	19	3.6
4	90 Dec. 28	12 : 27	4.9	64	153	—	20	1.5
5	91 Feb. 26	06 : 54	4.3	96	107	—	0.67	4.9
6	91 Apr. 24	09 : 32	5.4	52	146	147	75	1.9
7	91 June 13	05 : 11	6.0	123	133	—	510	0.61
8	91 June 17	01 : 52	3.8	69	94	—	1.3	3.3
9	91 June 20	00 : 07	4.1	61	89	—	2.6	3.3
10	91 June 23	20 : 38	4.8	67	125	156	32	2.2
11	91 June 27	07 : 53	4.6	73	116	—	7.3	5.9
12	91 Aug. 16	23 : 16	4.8	69	—	100	—	—
13	91 Sep. 02	12 : 03	5.0	65	—	93	—	—
14	91 Sep. 27	02 : 14	4.5	70	84	88	6.5	3.7
15	91 Oct. 18	01 : 57	5.3	56	174	—	35	2.8
16	91 Oct. 18	09 : 52	4.0	67	115	—	0.94	6.1
17	91 Oct. 25	19 : 39	6.1	104	173	150	210	1.7
18	91 Oct. 28	06 : 49	4.2	65	87	66	0.93	4.6
19	91 Nov. 02	10 : 44	4.0	62	158	—	1.1	5.3
20	91 Nov. 08	21 : 04	4.6	73	91	—	14	2.9
21	91 Nov. 11	20 : 15	4.8	63	—	141	—	—
22	91 Nov. 27	04 : 40	6.4	67	89	125	4,700	0.38
23	91 Dec. 03	06 : 32	3.7	56	81	—	0.64	4.9
24	91 Dec. 18	14 : 08	4.0	65	69	—	0.85	6.0
25	92 Jan. 12	11 : 37	4.0	44	46	—	1.3	5.4
26	92 Jan. 13	05 : 09	4.7	41	59	105	16	2.3
27	92 Jan. 17	03 : 47	5.4	75	161	—	97	1.2
28	92 Jan. 23	21 : 48	4.2	80	91	—	1.4	3.5
29	92 Jan. 26	03 : 39	4.2	49	98	—	5.9	1.7
30	92 Feb. 14	15 : 24	4.2	77	87	—	1.5	6.3
31	92 Mar. 02	21 : 19	4.8	71	113	143	24	3.5
32	92 Apr. 07	10 : 05	4.9	72	84	—	21	2.5
33	92 Apr. 20	05 : 36	5.0	62	64	97	8.8	3.3
34	92 July 12	20 : 09	6.3	65	152	193	750	0.61
35	92 July 13	23 : 19	5.3	71	153	—	87	1.3

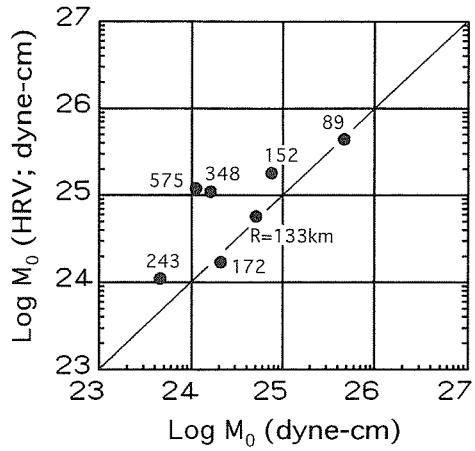

Fig. 7. Seismic moment M_0 obtained in this study and M_0 (HRV) from centroid moment tensor solution by the group of Harvard University. Solid line shows a relation of $M_0=M_0$ (HRV). The numerals indicate the hypocentral distance (R).

Table 2. Comparison of seismic moments obtained in this study. M_0 (MYR), and by the group of Harvard University M_0(HRV). H and R indicate the focal depth and the hypocentral distance.

No.	Date	Time	M	H (km)	R (km)	M_0(MYR) $\times 10^{24}$ dyn·cm	M_0(HRV) $\times 10^{24}$ dyn·cm
1	91 May 07	22 : 10	6.0	0	348	1.6	11
2	91 June 13	05 : 11	6.0	123	133	5.1	5.7
3	91 July 10	14 : 52	5.5	92	243	0.45	1.1
4	91 Oct. 08	12 : 32	6.1	144	575	1.1	12
5	91 Oct. 25	19 : 39	6.1	104	172	2.1	1.7
6	91 Nov. 27	04 : 40	6.4	67	89	47	44
7	92 July 12	20 : 09	6.3	65	152	7.5	18

selected events with the hypocentral distance of less than 200 km in this study as mentioned in section 2.

Figure 8 shows the relationship between M_0 and f_0 estimated. From this, we obtained the following relation:

$$\log M_0 = 24.3 - 2.95 \log f_0, \tag{2}$$

where M_0 is in dyne-cm and f_0, in Hz. This formula satisfies the power law relation of $M_0 f_0^3 =$ constant, and means that the Brune stress drop is about 200

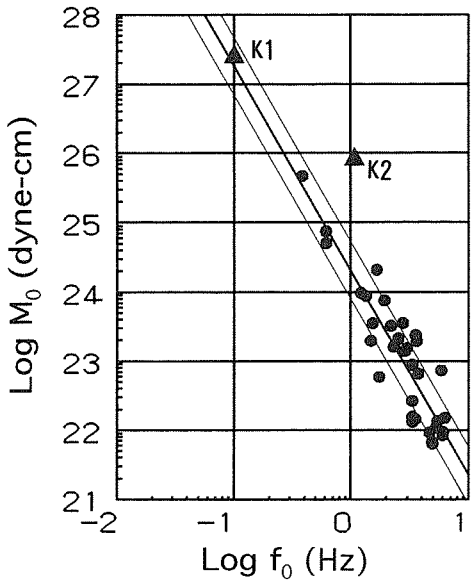

Fig. 8. Relation between seismic moments (M_0) and corner frequencies (f_0). Thick line indicates the M_0-f_0 relation from equation (2). Thin lines represent ±1 standard deviation about the relation. K1 and K2 show the relation between the first and second corner frequencies and the corresponding seismic moments for the 1993 Kushiro-Oki earthquake.

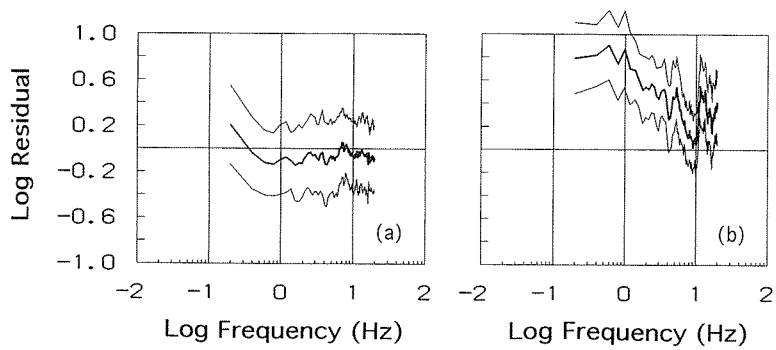

Fig. 9. Average residuals between the logarithms of the observed and model spectra. (a) MYR and (b) OUV. The thin lines represent the ±1 standard deviation.

bars irrespective of seismic moment. We also obtain the relationship between M_0 and M_{JMA} (JMA magnitude) as

$$\log M_0 = 1.34\, M_{JMA} + 16.7. \tag{3}$$

Here, we examine whether our spectral modeling by three parameters, M_0, f_0 and κ, fit the observed spectral shape. The model spectrum is calculated by using formula (1), and the relations of (2) and (3), giving M_{JMA} and R for each event. For κ values, we use their linear dependence on distances obtained by Mahdavian and Sasatani (1994):

$$\kappa(R) = 0.029 + 0.00014R, \tag{4}$$

where $\kappa(R)$ is in sec and R is in km. To measure the degree of fitness, we calculate the residual, RES(f), between the logarithms of the observed, $S(f)$, and model, $M(f)$, spectra at each frequency:

$$\mathrm{RES}(f) = \log S(f) - \log M(f). \tag{5}$$

Figure 9(a) shows the average and standard deviation of the residuals indicating good fitness between two spectra.

5. S-wave spectra for moderate-size events at the sedimentary site

We compare S-wave spectra at the sedimentary site, OUV, with those at the rock site, MYR, in Fig. 10. The OUV spectra at low frequencies are not flat, but have a peak in the frequency range from 0.1 to a few Hz, where the MYR spectra have a flat level. This indicates that the OUV spectra do not fit the omega-squared model. In this case, the application of the Andrews' method gives rise to erroneous estimates of the source parameters (Mahdavian, 1993).

Since the MYR spectra fit well the omega-squared model as mentioned in the previous section, the peak observed on the OUV spectra may be attributed to site response due to the sedimentary layer; beneath OUV station, the sedimentary thickness is about 1 km (Matsushima and Okada, 1990). We estimate the site response based on the residuals between the observed and model spectra following the method of Humphrey and Anderson (1992). The model spectrum is calculated using the same method as mentioned in the previous section. For κ values, we use their linear dependence on distances at OUV (Mahdavian and Sasatani, 1994):

$$\kappa(R) = 0.037 + 0.00019R, \tag{6}$$

where κ (R) is given in sec, and R, in km. The average of the residuals has

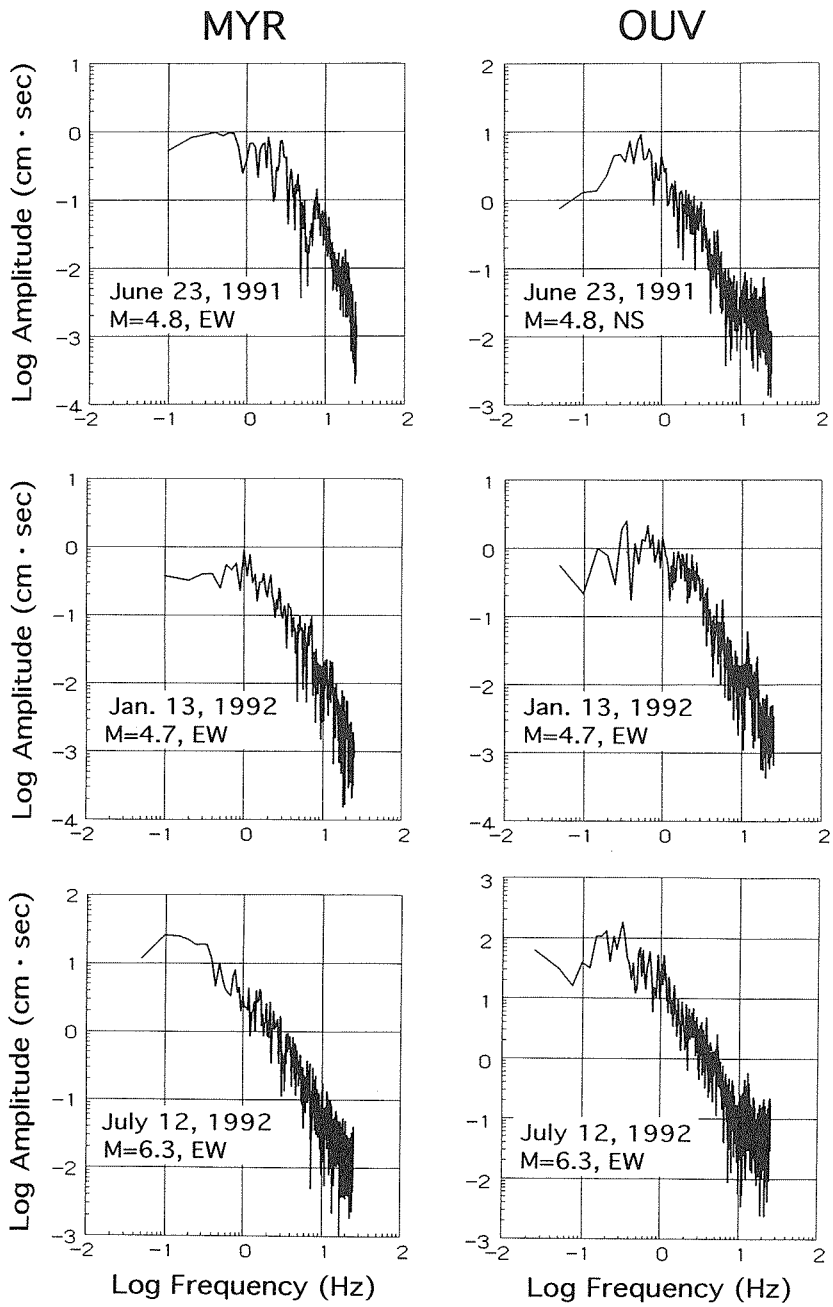

Fig. 10. Comparison between S-wave displacement spectra at MYR (left) and OUV (right) for moderate-size events.

large positive values (a factor of about 7) in the frequency range of 0.2 to 1 Hz as shown in Fig. 9(b).

6. The 1993 Kushiro-Oki earthquake

A destructive intermediate-depth (107 km) earthquake with a magnitude of 7.8 occurred on January 15, 1993, beneath Kushiro city, Hokkaido (inset in Fig. 11 and Table 3). This event provides a good opportunity to study the S-wave spectra for big events. Figure 11 shows observed velocity seismograms (horizontal components) at MYR and OUV. Unfortunately, the transverse (NS) component at OUV is off-scaled.

Figure 12(a) shows the S-wave spectrum (about 80 sec duration) at MYR for the transverse component. It is approximately flat at low frequencies of less

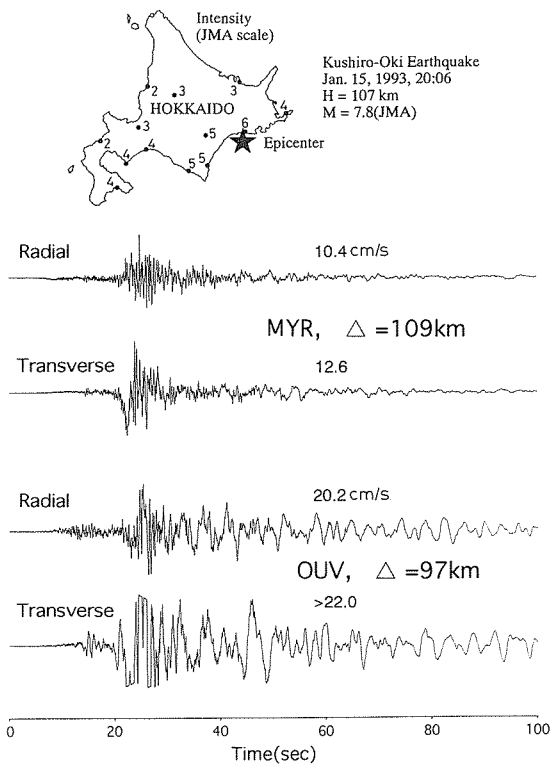

Fig. 11. Observed velocity seismograms at MYR and OUV from the 1993 Kushiro-Oki earthquake ($M=7.8$). The inset shows the epicenter of this big event.

Table 3. Focal parameters of the 1993 Kushiro-Oki earthquake and its aftershock.

	Date	Time	Lat. N	Long. E	M	H (km)
Main shock	93 Jan. 15	20 : 06	42°51′	144°23′	7.8	107
Aftershock	93 Feb. 04	23 : 43	42°57′	144°17′	4.9	95

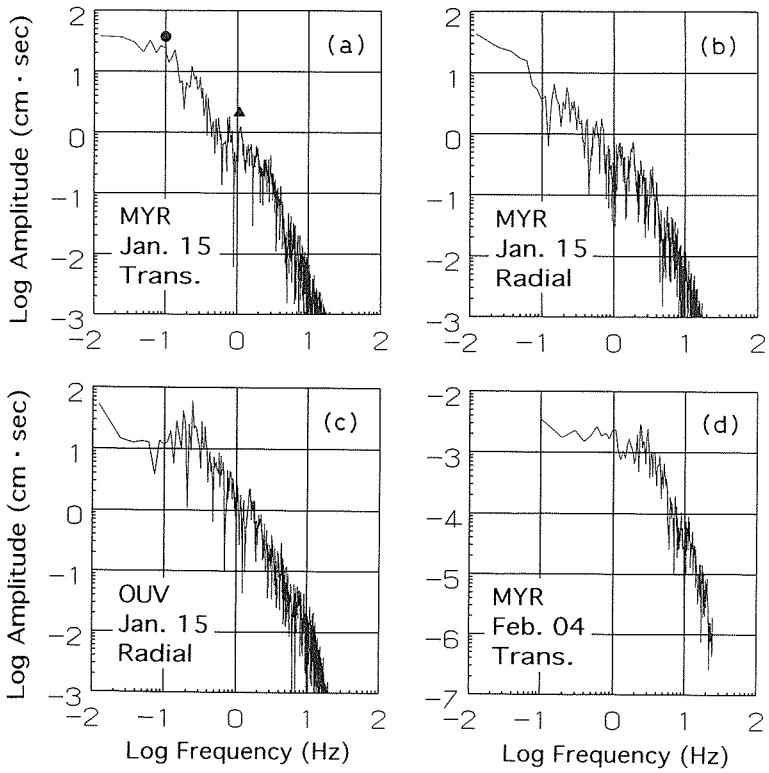

Fig. 12. (a) and (b): S-wave displacement spectra at MYR for the Kushiro-Oki earthquake. (c): S-wave displacement spectrum at OUV for the Kushiro-Oki earthquake. (d): S-wave displacement spectrum at MYR for an aftershock. In (a), a solid circle and a solid triangle represent the first and second corner frequencies.

than about 0.1 Hz and fall-off up to about 0.5 Hz in proportion to f^{-2}. The spectrum is rather flat in the frequency range of 0.5 to 1 Hz, and again fall-off in proportion to f^{-2} over about 1 Hz. We can identify two corner frequencies for this big event as shown in Fig. 12(a). The S-wave spectrum for the radial component at MYR is also shown in Fig. 12(b). Although the spectrum has not so clear flat level at low frequencies, it has nearly the same features as the transverse component spectrum.

For comparison, we show the spectrum for an aftershock with a magnitude of 4.9 (Table 3) in Fig. 12(d), which has approximately the same hypocenter as the main shock. It has only one corner frequency as discussed in section 4. This indicates that two corner frequencies on the big event spectra are not due to the wave propagation effect, but due to the source effect. Figures 12(a) and (b) show the observational evidence of a departure from the simple omega-squared model for this big event.

The OUV spectrum for this big event shows apparently one corner frequency (Fig. 12(c)). Here we note that the OUV spectra include the strong site response in the frequency range from 0.2 to 1 Hz as mentioned in the previous section. In fact, we can see the strong excitation of later phases with a period of a few seconds after S arrival on OUV records (Fig. 11). This site response obscures the existence of two corner frequencies as observed on the MYR

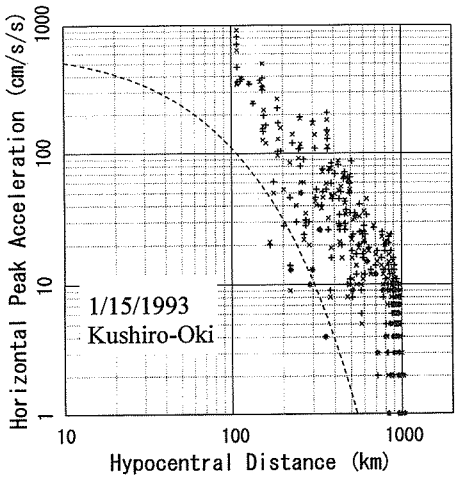

Fig. 13. Observed peak horizontal accelerations versus hypocentral distances during the 1993 Kushiro-Oki earthquake. A dashed curve indicates the empirical relation for $M=7.8$ event based on Fukushima and Tanaka (1990).

spectra. The OUV spectrum corrected for the site response in Fig. 9(b) may depict two corner frequencies.

We cannot apply the Andrews' method to estimate the source parameters for this big event, because his method is based on the omega-squared model. Thus we visually estimate the first (f_0) and second (f_0*) corner frequencies and evaluate the corresponding seismic moments (M_0 and M_0*) based on the MYR transverse component spectrum. These values are: $f_0=0.1$ Hz, $M_0=2.5\times10^{27}$ dyne-cm, $f_0{}^*=1.1$ Hz and $M_0{}^*=7.5\times10^{25}$ dyne-cm. The seismic moment M_0 is approximately the same as that (3.3×10^{27} dyne-cm) obtained by Takeo et al. (1993), but somewhat smaller than the HRV solution (6.8×10^{27} dyne-cm). Our estimates of M_0 and f_0 lie on the scaling law (2) as shown in Fig. 8.

The seismic moment corresponding to the second corner frequency is much larger than that estimated based on the obtained scaling law as shown in Fig. 8. This indicates that the Kushiro-Oki earthquake radiates abnormally strong short-period seismic waves. In fact, observed horizontal peak accelerations are much higher than those predicted by an empirical attenuation relation, as shown in Fig. 13. Takeo et al. (1993) studied the source process of the Kushiro-Oki earthquake using near-field data and characterized this event by a high stress drop event in a subducting slab. This study and our findings may indicate that the high stress drop event has the S-wave spectrum with two corner frequencies and radiates abnormally strong short-period seismic waves.

7. Discussion and conclusions

We analyzed S-wave spectra from strong motion seismograms and obtained source parameters (M_0 and f_0) for 32 moderate-size events and for one big event. The relation between M_0 and f_0 for moderate-size events given by equation (2) indicates the Brune stress drop of about 200 bars. This stress drop is approximately the same as that for events of $M<6$ off Fukushima Prefecture (Takemura et al., 1993) and for events in active extensional area in Italy (Rovelli et al., 1988), but larger than that for local events in California (Hanks and McGuire, 1981). For $M>6$ events, Takemura et al. (1993) obtained another M_0-f_0 relation, which is consistent with the M_0-f_0 relation for $M7$ to 8 shallow events in the world with the stress drop of about 30 bars (Houston and Kanamori, 1986). However, our results show that the equation (2) is valid for a wide magnitude range from 4 to 8 as shown in Fig. 8. Here we note that focal depths of $M>$ 6 events analyzed by Takemura et al. (1933) are 30 to 50 km, which are shallower than those (60-120 km) of $M>6$ events analyzed here. Thus the different M_0-

f_0 relations for events off Fukushima and in the southern part of Hokkaido may be due to regional and/or depth variations of the relation.

Source spectra of complex earthquakes are characterized by two corner frequencies (e.g., Koyama, 1983 ; Papageogiou and Aki, 1983). Many previous studies have shown two corner frequencies in a wide magnitude range ($M=4$-7) and in various regions (e.g., Izutani, 1984 ; Koyama, 1983 ; Papageogiou, 1988 ; Takemura et al., 1993). Recently, Takemura et al. (1993) identified two corner frequencies on the source spectra for $M>6$ events off Fukushima Prefecture, Japan, but in this study, we identified only one corner frequency even for $M>$ 6 events (see Fig. 5), except the 1993 Kushiro-Oki event ($M=7.8$). These results may indicate the regional variation of complex faulting.

From a review of the previous results, Takemura et al. (1993) have shown that the second corner frequency is at about 1 Hz as an average for M6 class events, in spite of large regional variations. The second corner frequency of the Kushiro-Oki big event is about 1 Hz which is almost consistent with that for M6 class events. This may imply approximately the same average scale length of the fault heterogeneities despite the different magnitude, focal depth, and region.

As shown in Figs. 10 and 12, the S-wave spectra at the sedimentary site (OUV) are different from those at the rock site (MYR). We interpreted this difference as the site response. Figure 9(b) shows the strong amplification at relatively low frequencies (0.5 to 1 Hz) at OUV. The observed seismograms at OUV have strong later phases as shown in Figs. 5 and 11. These later phases are basin-induced surface waves (Furumura and Sasatani, 1995). Thus, the site response in Fig. 9(b) includes not only amplification due to thick sedimentary layer but also effects of the basin-induced surface waves.

Acknowledgments

We thank Dr. M. Furumura of our laboratory and Professor T. Koyanagi of Obihiro University for their cooperation in strong motion observations at MYR and OUV.

References

Aki, K., 1967. Scaling law of seismic spectrum. J. Geophys. Res., **72**, 1217-1231.

Anderson, J.G. and S. Hough, 1984. A model for the shape of the Fourier amplitude spectrum of acceleration at high frequencies. Bull. Seism. Soc. Am., **74**, 1969-1994.

Andrews, D.J., 1986. Objective determination of source parameters and similarity of earthquakes of different size. in Earthquake Source Mechanics, S. Das, J. Boatwright, and C.H. Scholz (Editors), American Geophysical Union, Washington, D.C., 259-268.

Boore, D.W., 1983. Stochastic simulation of high-frequency ground motions based on seismological models of the radiated spectra. Bull. Seism. Soc. Am., **73**, 1865-1894.

Brune, J.N., 1970. Tectonic stress and the spectra of seismic shear waves. J. Geophys. Res., **75**, 4997-5009.

Dobry, R., M. Idriss and E. Ng, 1978. Duration characteristics of horizontal components of strong-motion earthquake records. Bull. Seism. Soc. Am., **68**, 1487-1520.

Dziewonski, A.M. and J.H. Woodhouse, 1983. An experiment in systematic study of global seismicity : central-moment tensor solutions for 201 moderate and large earthquakes of 1981. J. Geophys. Res., **88**, 3248-3271.

Fukushima, Y. and T. Tanaka, 1990. A new attenuation relation for peak horizontal acceleration of strong earthquake ground motion in Japan. Bull. Seism. Soc. Am., **80**, 757-783.

Furumura, M. and T. Sasatani, 1995. Secondarily generated surface waves in the Tokachi basin, Hokkaido, Japan. J. Phys. Earth (in press).

Geological Survey of Hokkaido, 1980. Geological map of Hokkaido (1 : 600,000).

Hanks, T.C. and R.K. McGuire, 1981. The character of high-frequency strong ground motion. Bull. Seism. Soc. Am., **71**, 2071-2095.

Houston, H. and H. Kanamori, 1986. Source spectra of great earthquakes : teleseismic constraints on rupture process and strong motion. Bull. Seism. Soc. Am., **76**, 649-674.

Humphrey, J.R. and J.G. Anderson, 1992. Shear-wave attenuation and site response in Guerrero, Mexico. Bull. Seism. Soc. Am., **82**, 1622-1645.

Iwata, T. and K. Irikura, 1988. Source parameters of the 1983 Japan Sea earthquake sequence. J. Phys. Earth, **36**, 155-184.

Izutani, Y., 1984. Source parameters relevant to heterogeneity of a fault plane. J. Phys. Earth, **32**, 511-529.

Koyama, J., 1983. Earthquake source spectrum from coherent and incoherent rupture on a fault. Zisin, Ser. 2, **36**, 225-235 (in Japanese with English abstract).

Mahdavian, A., 1993. A study of the characterization and predictive modeling of strong ground motion during earthquakes around Hokkaido, Japan. Ph.D. Thesis, Hokkaido University, pp. 113.

Mahdavian, A. and T. Sasatani, 1994. Spectral shape of acceleration at high frequencies : Attenuation and site effect. J. Fac. Sci. Hokkaido Univ., Ser. VII (Geophys.), **9**, 415-427.

Matsushima, T. and H. Okada, 1990. Determination of deep geological structure under urban areas using long-period microtremors, BUTSURI-TANSA, **43**, 21-33.

Muramatu, I., 1977. A velocity type strong motion seismograph with wide frequency range. Zisin, Ser. 2, **30**, 317-338 (in Japanese with English abstract).

Muramatu, I., 1995. Development of a broadband velocity type strong motion seismometer and its recording range. Zisin, Ser. 2, **48**, 247-256 (in Japanese with English abstract).

Papageorgiou, A.S., 1988. On two characteristic frequencies of acceleration spectra : patch corner frequency and fmax. Bull. Seism. Soc. Am., **78**, 509-529.

Papageorgiou, A.S. and K. Aki, 1983. A specific barrier model for the quantitative description of inhomogeneous faulting and the prediction of strong ground motion. I. Description of the model. Bull. Seism. Soc. Am., **73**, 693-722.

Rovelli, A., O. Bonamassa M. Cocco, M.D. Bona, and S. Mazza, 1988. Scaling laws and spectral parameters of the ground motion in active extensional area in Italy. Bull. Seism. Soc. Am., **78**, 530-560.

Sasatani, T., T. Matsushima and T. Koyamagi, 1990. Observation of strong ground motion in

and around the Tokachi plain. Geophys. Bull. Hokkaido Univ., **54**, 15-22 (in Japanese with English abstract).

Takemura, M., K. Kato, T. Ikeura and E. Shima, 1991. Site amplification from strong motion records in special relation to surface geology. J. Phys. Earth, **39**, 537-552.

Takemura, M., T. Ikeura and T. Uetake, 1993. Characteristics of source spectra of moderate earthquakes in a subduction zone along the Pacific coast of the southern Tohoku district, Japan. J. Phys. Earth, **41**, 1-19.

Takeo, M., S. Ide and Y. Yoshida, 1993. The 1993 Kushiro-Oki, Japan earthquake: A high stress-drop event in a subducting slab. Geophys. Res. Letters, **20**, 2607-2610.